International Journal of Mass Spectrometry 476 (2022) 116834

Contents lists available at ScienceDirect

International Journal of Mass Spectrometry

journal homepage: www.elsevier.com/locate/ijms

Similarities and dissimilarities in the fragmentation of polycyclic aromatic hydrocarbon cations: A case study involving three dibenzopyrene isomers

Helgi Rafn Hrodmarsson [a, *], Jordy Bouwman [a, b, c, d], Alexander G.G. M. Tielens [e], Harold Linnartz [a]

[a] Laboratory for Astrophysics, Leiden Observatory, Leiden University, PO Box 9513, NL-2300, RA Leiden, the Netherlands
[b] Laboratory for Atmospheric and Space Physics, University of Colorado, Boulder, CO, USA
[c] Department of Chemistry, University of Colorado, Boulder, CO, USA
[d] Institute for Modeling Plasma, Atmospheres, and Cosmic Dust (IMPACT), NASA/SSERVI, Boulder, CO, USA
[e] Leiden Observatory, Leiden University, PO Box 9513, NL-2300RA Leiden, The Netherlands

ARTICLE INFO

Article history:
Received 12 November 2021
Received in revised form
23 February 2022
Accepted 4 March 2022

ABSTRACT

The photon induced fragmentation behavior of the cations of three dibenzopyrene ($C_{24}H_{14}$) isomers (DBPae, DBPah and DBPal) is studied in a series of systematic mass spectrometric experiments. The ions are collected in an ion trap system and irradiated with different numbers of photons before being released into a time-of-flight mass spectrometer. The resulting mass spectra show a number of remarkable similarities, despite the structural differences between the three precursor species. Differences in the fragmentation patterns are found as well. Whereas it is not straight forward to explain the molecular origin of these findings, it is clear that the observed fragmentation patterns are relevant to further interpret the molecular composition of the interstellar medium (ISM), in which PAHs are omnipresent and subject to intense radiation. The main conclusion of this work is that PAHs comparable to the one studied here, may enrich the ISM with pure carbon species, C_n^+, with n values roughly between 11 and 15, following a top-down approach.

1. Introduction

Polycyclic aromatic hydrocarbons (PAHs) are widely accepted as the carriers of the aromatic infrared bands (AIBs) which are observed towards a multitude of interstellar objects [1]. PAHs likely originate in the outflows of AGB stars at the end of their lives [2]. With the recent unambiguous radio astronomical detections of the first individual PAHs in the denser interstellar medium (ISM), towards Taurus Molecular Cloud (TMC-1) [3–5], important steps have been made in understanding the cosmochemical evolution of PAHs. At the same time, much about the chemical behavior of PAHs in the ISM is still far from understood. In addition, PAHs and their derivatives may be omnipresent in the diffuse ISM, acting as potential molecular carriers of the diffuse interstellar bands (DIBs) which have remained a spectroscopic mystery for a century now [6–8].

Individual PAHs have been invoked as potential DIB carriers in a multitude of studies [9–12] but none have been definitively assigned so far. Recently, C_{60}^+ has been confirmed as the carrier of 4 of the DIBs [13–15]. The presence of C_{60}^+ in the diffuse interstellar medium may not be all that surprising, though, given the detection of C_{60} in other ISM regions [16,17], and considering that the C_{60}^+ cation is known to start fragmenting at 50 eV [18], which is a significantly higher energy threshold than interstellar photons are capable of overcoming. Among the most prominent theories concerning the interstellar origins of fullerenes is the photo-induced dehydrogenation and subsequent bowling of large PAHs [19,20] which has been confirmed as a viable possibility in the laboratory [21]. This is further backed with the observation of a clear trend for decreasing PAH abundances and an increase in C_{60} abundances with stronger radiation fields [20,22]. This is a strong indicator that the formation of fullerenes follows a top-down mechanism. A key element in the top-down mechanism is a bowling process that

* Corresponding author.
E-mail addresses: hrodmarsson@strw.leidenuniv.nl, hr.hrodmarsson@gmail.com (H.R. Hrodmarsson).

https://doi.org/10.1016/j.ijms.2022.116834

involves the formation of pentagons [23,24]. It was shown that these also form effectively in a bottom-up mechanism that also may contribute to the formation of fullerenes or carbon cages as well [25].

These formation routes are in line with the GRANDPAH hypothesis [26,27]. The GRANDPAH hypothesis states that a limited number of compact, highly symmetric PAHs dominate the interstellar PAH family at the brightest spots of UV-rich regions, meaning that other, less stable PAHs that were present, are destroyed or transformed into more stable species by photons, collisions, dissociative recombination, *etc*. This raises the question whether continued irradiation and fragmentation of PAHs could also lead to other fragments that are exceedingly stable, such as C_{60}^{+}, that could survive for eons in the diffuse interstellar medium and for this reason also would be good carrier candidates of the elusive DIBs. It has been suggested that the photolysis of PAHs in UV-rich regions may also contribute to the organic inventory of small hydrocarbon species in such regions [28].

Much experimental and theoretical work has been devoted to the fragmentation of PAHs and it is well-documented that PAH mass spectrometric behavior is "unusual" [29–31]. Characterizing the importance of PAH isomers has especially received attention and many studies report that the fragmentation of PAH isomers appears to follow identical or very similar pathways [23,24,27,32–40] though some nuances have also been reported which include the competition between losses of atomic H and molecular H_2 for a variety of PAH structures [41].

Thus, we present here a case study of the photo-induced fragmentation of three PAH isomers of dibenzopyrene (DBP), $C_{24}H_{14}$, of different symmetries that would be unlikely survivors in photon dominated regions. These are dibenzo[a,e]pyrene (DBPae, C_s), dibenzo[a,h]pyrene (DBPah, C_{2h}), and dibenzo[a,l]pyrene (DBPal, C_1) (see Fig. 1); each of which possessing clearly different molecular symmetries. In Ref. [42], the gas phase IR spectra of their cationic species were presented. The number of IR active bands increases as the symmetry of the molecule lowers, as expected. Prior studies of the interaction of DBPae and DBPal with VUV synchrotron radiation revealed that the level of fragmentation of these two isomers are similar from 13 eV to 20 eV, but the onset of fragmentation is lower for DBPal than for DBPae [43]. The initial H/H_2 loss in these two isomers was further investigated with density functional theory [44] to reveal that DBPal preferentially loses the two out-of-plane H atoms in either one or two steps, both of which are more easily accessed via lower barriers than the initial H/H_2 loss in DBPae. One key question that requires further study is if (and how) molecular symmetry affects the fragmentation channels.

Our results reveal that there are important and perhaps universal similarities in their breakdown products, despite the different geometrical properties, but also subtle dissimilarities that require deeper studies into continued PAH fragmentation/excitation. The work presented here also links to the GRANDPAH hypothesis [26], namely that besides the GRANDPAHs themselves, stable products of PAH fragmentation (whether produced by means of VUV photons, X-rays, dissociative recombination, energetic collisions, etc.) might be more important than the PAH precursor species. Such fragments may act as molecular carriers of the more than 500 unassigned DIBs. In the present mass spectrometric study, we assess if PAH fragments of certain masses are generally (more) favored.

2. Methodologies

2.1. Experimental set-up

The experiments were performed on the 'instrument for Photodynamics of PAHs' (i-POP), situated in the Laboratory for Astrophysics (LfA) at Leiden observatory. i-POP has been described in detail elsewhere [45] so only the relevant details are given here. The apparatus consists of two differentially pumped chambers; a source chamber that houses a commercially available ion trap (Jordan C-1251), and a detection chamber which comprises a reflectron time-of-flight spectrometer (Jordan D-850). The three DBP samples are commercially available from Chiron (DBPae 99.5%, DBPah 99.8%, DBPal 99.5%). The samples were evaporated in the source chamber using a Heat Wave Labs built oven held at around 92°C. The sample vapors were ionized by an electron ionization at 84 eV using an electron gun (EGUN, Jordan C-950) and the resulting cations were subsequently guided into the ion trap through an electrostatic ion gate.

For these measurements, we used 2000 V top-top RF signal on the ring electrode at an operating frequency of 1.25 MHz in the ion trap to retain ions and this translates to the trap retaining masses from approx. 120 amu up to several hundred amu. Helium buffer gas was admitted up to a static pressure of $1–2 \times 10^{-6}$ mbar in the source chamber. Through collisions with helium, the PAH cations were confined to the center of the ion trap [46,47] and remained there until the sample was guided from there into the detection chamber. While caught in the center of the trap, the ions were irradiated with a nanosecond pulsed Quanta-Ray Nd:YAG laser (DCR2A-3235) pumping a dye laser (LIOP-TEC, Quasar2-VN) which was set to deliver 620 nm photons. The laser was horizontally guided through the ion trap and was operated at 10 Hz to irradiate the trapped ions.

The reasoning for the choice of 620 nm laser radiation was the following. As the ultimate objective of the experiment was to "scan" over the potential energy surface of the three DBP molecules, the

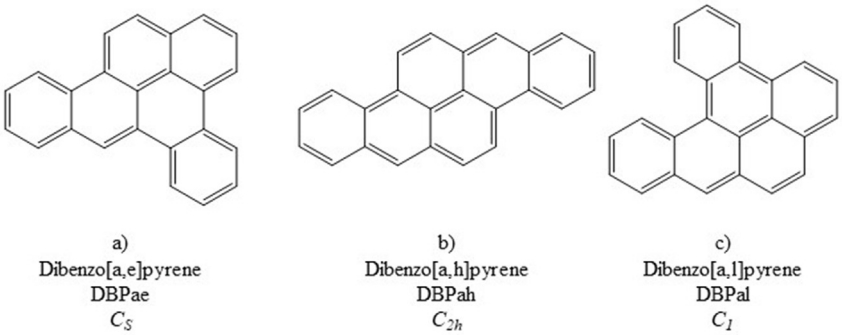

Fig. 1. Molecular structures of the three $C_{24}H_{14}$ (302 amu) dibenzopyrene isomers considered in this work. We also list their respective abbreviated names used throughout this article and their symmetry point groups.

choice of 620 nm laser radiation allowed us to minimize multiple ionization, which DBPae and DBPal are known to do in competition with fragmentation with VUV photons [43,48]. Hence using longer wavelength photons in a multi-photon process allowed us to obtain more information about the molecules' fragmentation patterns in a gentler manner to elucidate more nuanced differences in the fragmentation patterns.

The timing sequences of the data acquisition cycle were controlled by a high-precision delay generator (SRS DG535), which was triggered by the Nd:YAG laser's Q-switch timing to ensure synchronization at the start of each measurement cycle. Each operation cycle consisted of filling of the ion trap, mass isolation of the parent ion, irradiation of the ion cloud, and ejecting the ions into the TOF tube. The scan cycle began with an empty ion trap and was initiated with the opening of the ion gate, filling the ion trap for a duration of 2 s. Shortly thereafter (ca. 0.2 s) the ions had thermalized through collisions with the He buffer gas which led to the cloud shrinking. To isolate the masses of the parent PAH ions, a ca. 65 ms long Stored Waveform Inverse Fourier Transform (SWIFT) pulse was applied to one of the end caps of the ion trap in order to isolate the parent species [49]. It should be noted that the harsh electron impact ionization source not only produced parent PAH cations but fragments due to e.g., C_2H_2, and H_2 loss as well. For the purposes of this work, the SWIFT pulse was applied to isolate the parent cations as well as the cations corresponding to H_2 losses from the parent (i.e., the 298−304 amu range) and effectively filter out other spurious signals or losses due to, *e.g.*, C_2H_2. After the SWIFT pulse was employed, the laser beam shutter was opened and the ion cloud was irradiated. At the end of the irradiation time, the ions were accelerated out of the trap and into the field-free TOF region at the end of which the ions were detected by a multichannel plate detector and digitized using a FASTCOM time binning card.

2.2. Mass spectra analysis and visualization

A number of data acquisitions were performed where the laser power and the number of laser pulses were varied. Namely, so-called acquisition 'trains' were performed with 3.5, 5.0, and 6.5 mJ energies per laser pulse (which equates to a flux of approx. 35, 50, and 65 mJ/cm^2/pulse), with the following numbers of pulses: 1, 2, 3, 4, 5, 10, 15, and 20. These numbers of pulses were chosen such that the majority of the parent DBP cation species would be depleted in the ion trap and converted to fragments. In each case, the total cycle duration was kept constant at 5 s to ensure that all datasets are cross comparable and the only changed parameter is pulse energy and/or number of pulses. In the case of DBPal, an additional pulse train was recorded using 6.5 mJ/pulse and the following number of pulses: 10, 20, 30, 40, 50, 60, and 70 (with a total duty cycle of 10 s) such that the (dehydrogenated) parent species ($C_{24}H_x$, x = 0−12) achieved the same level of depletion as in DBPae and DAPah.

Each recorded mass spectrum was treated with a three-point smoothing function. The data analysis and visualization program IGOR Pro was used for analysis utilizing the built-in multi-peak function to fit the mass peaks that were of particular interest. Gaussian fits were used to derive peak areas as they gave satisfactory fits with absolute errors of 5% or less. In addition, to account for the uncertainty of the absolute number of ions in the trap from fill to fill, additional reference spectra were recorded between each laser measurement with the laser turned off. For one measurement train the average of the peak areas of the parent recorded with the laser off was used to calibrate the peak areas of that particular train. On average these gave errors in the 2−8% range. Error propagation leads to an approximate 10% absolute error in the normalized peak areas presented in section 3.

To further assist the data visualization and analysis, TOF-MS matrices were constructed by concatenating the trains of mass spectra recorded by using the same laser pulse energies, but different numbers of laser pulses within each measurement cycle. In Fig. 2 it is illustrated how the mass signals for different pulses can be summarized in a color diagram. Thus, the y-axis in each matrix equals the number of laser pulses, the x-axis is the *m*/*z* ratio, and the color intensity is the intensity of the mass peaks. Prior to concatenation, the baseline was subtracted from each mass spectrum to minimize noise in the TOF-MS matrix.

The matrix allows us to clearly identify which fragmentation channels are the most important and which mass fragments are the most stable upon continued irradiation by the laser. This gives us insight into which fragments are accessed at lower energies, which fragments form at higher energies, or approximate energy windows through which the fragments are only accessible. The resulting matrices show clearly the depletion of the parent species in question, and the formation of important intermediates that will be discussed in the Results and Discussion sections.

3. Results

3.1. Mass spectra

3.1.1. Dibenzo[a,e]pyrene (DBPae)

Fig. 3 presents the TOF-MS matrices of DBPae for three different pulse energies: 3.5, 5.0, and 6.5 mJ/pulse. Inspection of the top panel of Fig. 3 (3.5 mJ/pulse) allows us to decipher a number of interesting fragmentation pathways. Furthermore, in the structural geometries listed below it is not always indicated that a fragment is in fact cationic as otherwise it would not be detectable through ion trap TOF mass spectrometry. At the end of this section, the numbers of laser pulses required to open up the most relevant fragmentation channels of the three DBP isomers are summarized in Table 1.

First, unlike several other larger PAHs, DBPae does not fully dehydrogenate prior to losing one or two carbon atoms [34,36]. Rather, after one, two, and three losses of H_2 (or alternatively two sequential H atoms [44]), the molecule then loses C_2H_2 fragments (or alternatively, sequential H_2/2H and C_2 losses − it is impossible to distinguish between the two from these data) corresponding to fragments at 270, 272, and 274 amu ($C_{22}H_6$, $C_{22}H_8$, and $C_{22}H_{10}$, respectively). The next fragments that are formed appear to be those at 246 and 248 amu ($C_{20}H_6$ and $C_{20}H_8$) which correspond to the loss of a second C_2H_2/H_2+C_2 fragment/s from the $C_{22}H_8$ and $C_{22}H_{10}$ fragments, respectively. A third loss of C_2H_2 (from the $C_{20}H_8$ fragment) appears at 222 amu ($C_{18}H_6$), but for the 3.5 mJ/pulse train of mass spectra, this fragment is quite weak. The DBPae cation can ultimately fully dehydrogenate but fragments breaking off the carbon skeleton are more easily formed (*i.e.* by using fewer laser pulses).

Also observed is the loss of CH as evidenced by the mass peaks found at the odd-numbered 281, 283, and 285 amu masses ($C_{23}H_5$, $C_{23}H_7$, and $C_{23}H_9$, respectively). These correspond to the loss of CH from DBPae that has already lost six, five, and four H_2 units, respectively. This seems to be an indication that DBPae requires further H_2 loss for CH loss to occur than for the loss of C_2H_2. And further, the loss of C_2H_2 is energetically favored prior to complete dehydrogenation. We will cautiously discount losses of CH_3 as such losses have only been observed for (partly) hydrogenated PAHs [37]. A CH_3 fragment requires the formation of a sp^3 hybridized carbon atom and the migration of two hydrogen atoms to the same carbon atom. Although H-migration has been found to be a quintessential pathway for H_2 losses from PAHs [41,50,51], we anticipate a loss of CH_3 preceded by two separate H-migrations to the same carbon atom to be of minor significance for the time being.

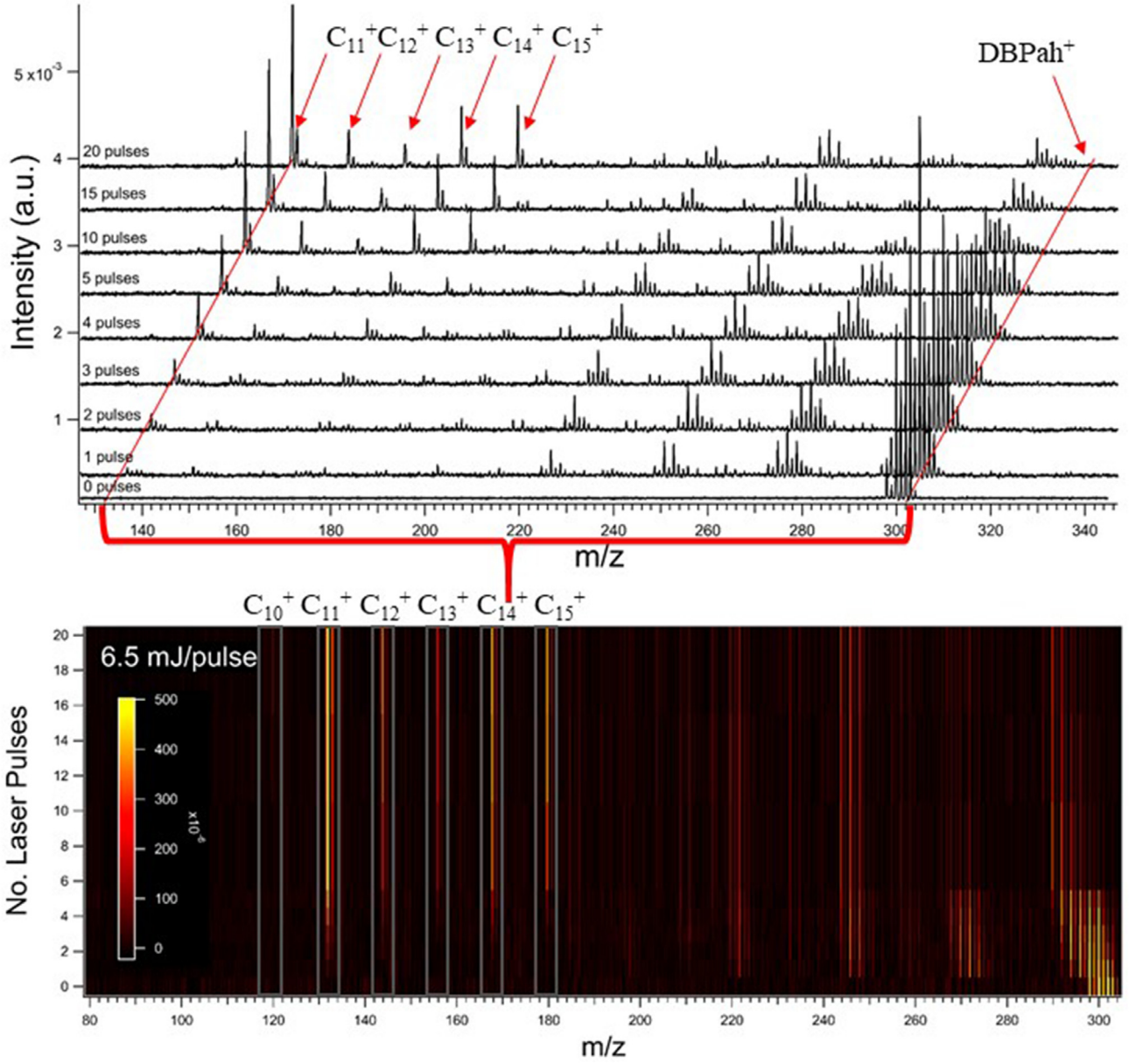

Fig. 2. Construction of a TOF-MS matrix for DBPah. The mass spectra in the upper panel are shifted up and to the right to show the evolution of the mass signals with increasing laser irradiation. The red diagonal lines follow the locations of the parent cation and the C_{11}^{+} signals in the mass spectra. Each TOF-MS corresponds to a measurement with the number of pulses varying from 0 to 20. The signal intensities are given in arbitrary units as the baseline needs to be corrected in each individual mass spectrum. After correction for the baseline, the mass spectra are concatenated to form the TOF-MS matrix in the lower panel. The color scale is for all the TOF-MS matrices is kept the same for consistency. Lower panel also highlights where the C_{10}^{+} - C_{15}^{+} carbon clusters appear.

Perhaps the most visually striking aspect of these mass spectra is the facile and early formation of the C_{11}^{+} carbon clusters. Their appearance seems to be favored after the third C_2H_2 (or C_2+H_2) loss. This could be an indication that H_2-loss and a further loss of three C_2H_2 units is required for the facile formation of C_{11}^{+} from the DBPae parent. At higher pulse energies, the C_{14}^{+} and C_{15}^{+} carbon clusters become apparent albeit weakly, but their formation appears to come after the loss of a CH unit, a few H_2 units, and sequential C_2H_2 units. This is, however, difficult to discern. One more interesting thing to note is the C_{11}^{+}, C_{14}^{+} and C_{15}^{+} signals are not accompanied by a $C_nH_2^{+}(n = 11, 14, 15)$ signal while the C_{10}^{+}, C_{12}^{+} and C_{13}^{+} signals are. At this point it is important to note that because the signal pertaining to C_{10}^{+} is right at the cutoff of the stability region of the ion trap, we refrain from drawing any conclusions about its signal or lack thereof in the mass spectra shown in Fig. 3 and later figures.

When we inspect the mass signals corresponding to the fragmentation from the use of 5.0 mJ/pulse laser energies (middle panel of Fig. 3), many of our suppositions seem to be further supported. Again, the losses of C_2H_2 from a partly dehydrogenated DBPae parent cation ($C_{24}H_x$, x = 0–8; signals between 288 and 296 amu) are favored over (or accessed at lower energies than) the loss of CH ($C_{23}H_x$, x = 5–12; signals between 281 and 288 amu).

Besides C_{11}^{+}, the appearance of C_{12}^{+}, C_{14}^{+} and C_{15}^{+} is also observed (and to a lesser degree C_{13}^{+}). Interestingly, the initial appearances of the C_{12}^{+} and C_{14}^{+} mass signals are accompanied by doubly hydrogenated mass signals corresponding to $C_{12}H_2^{+}$ and $C_{14}H_2^{+}$. Likewise, it appears that C_nH^{+} are formed as their peaks are generally a little

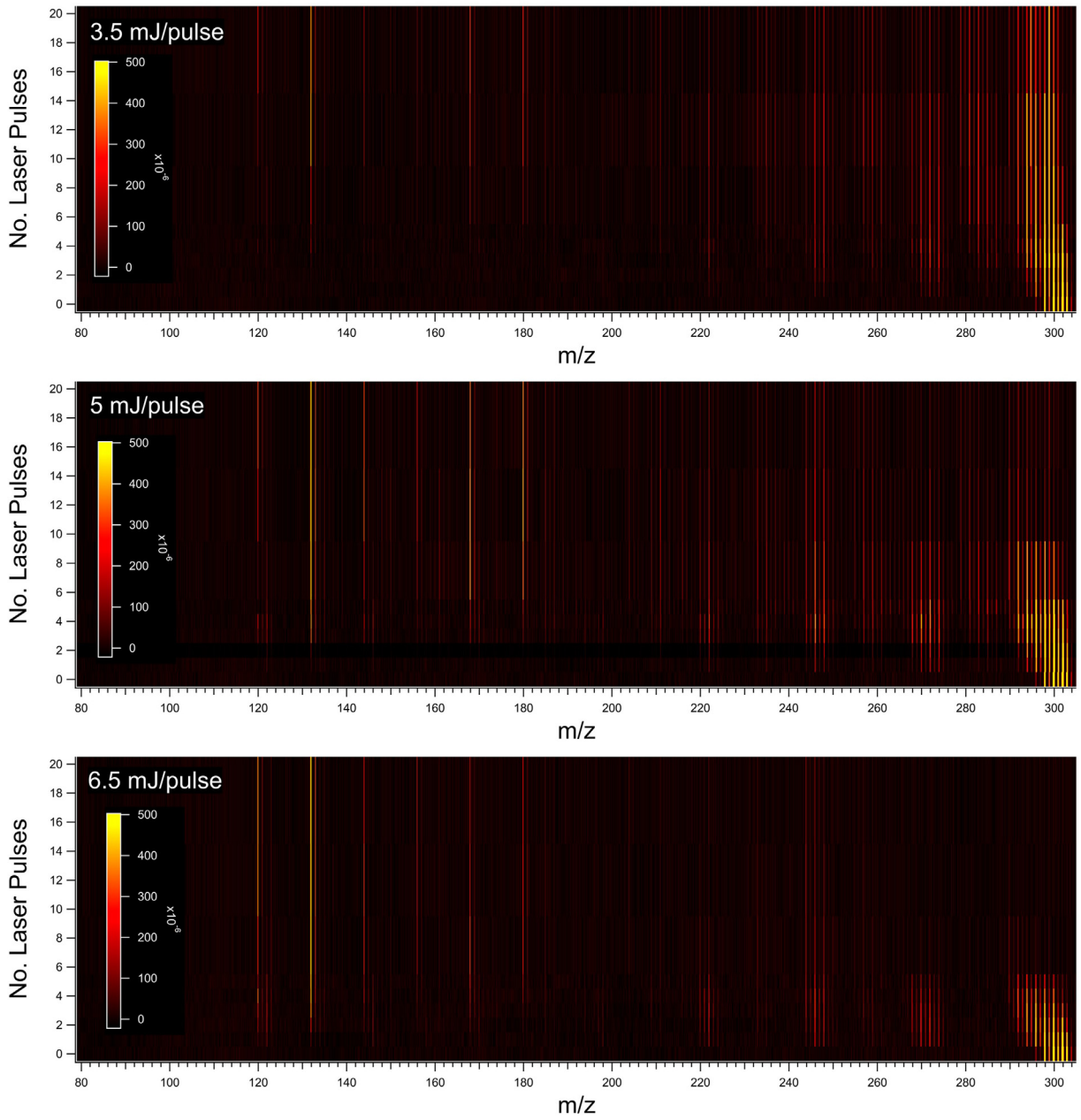

Fig. 3. Two-dimensional TOF-MS representation of the laser-induced photofragmentation of DBPae cation. Each panel shows the number of laser pulses on the y-axis, the *m/z* ratio on the x-axis and the color scale indicates the strength of the mass peaks.

larger than the expected ^{13}C contribution from the parent C_nH^+ peaks. In all cases, however, these doubly hydrogenated masses disappear when 10 pulses or more are used to irradiate the ion cloud. This could be a strong indicator that the precursor of these carbon clusters can break off the parent PAH molecule with two hydrogens before quickly losing them upon further irradiation.

Another intriguing aspect is that of the signals corresponding to two C_2H_2 losses after one, two, or three H_2 losses from the DBPae parent (signals at 244, 246, and 248 amu corresponding to $C_{20}H_2$, $C_{20}H_4$, and $C_{20}H_6$, respectively). As the continued irradiation depletes the signals corresponding to other losses (i.e., loss of a single C_2H_2 unit, loss of three C_2H_2 units as well as the losses of a CH unit and *n* x C_2H_2 units), the $C_{20}H_2$, $C_{20}H_4$, and $C_{20}H_6$ signals appear to persist despite the ongoing laser irradiation. This indicates that these reaction products may play an important role as intermediates in the fragmentation of DBPae where they are both easily formed and relatively easily destroyed to form other more stable fragments like *e.g.*, the observed carbon clusters.

If we inspect the mass signals corresponding to the fragmentation from the use of 6.5 mJ/pulse laser energies (bottom panel of Fig. 3) we see that while all the masses corresponding to the losses of various C_2H_2 and/or CH units are entirely depleted, the $C_{20}H_2$, $C_{20}H_4$, and $C_{20}H_6$ mass peaks are still present at the highest levels of irradiation.

And finally, at 6.5 mJ/pulse and 20 pulses, the C_{11}^+, C_{12}^+, C_{13}^+, C_{14}^+ and C_{15}^+ mass peaks are still present, i.e., not depleted, with the C_{11}^+ species the most prominent by a significant degree.

3.1.2. *Dibenzo[a,h]pyrene (DBPah)*

Fig. 4 presents the TOF-MS matrices of DBPah which correspond to the same concatenations of mass spectra as those of DBPae presented in Fig. 3. The first thing to note is that DBPah does not

undergo complete dehydrogenation prior to losing one or two carbon atoms from the carbon backbone, just like the DBPae isomer. The highest level of dehydrogenation observed is above the use of five 3.5 mJ pulses where a signal at 290 amu is observed, which corresponds to the retention of two H atoms to the carbon skeleton, $C_{24}H_2^+$.

Secondly, the CH loss from DBPah is somewhat weaker than in DBPae and it is C_2H_2 loss that appears to be the dominant fragmentation pathway as evidenced by the strong signals at 270, 272, and 274 amu ($C_{22}H_6$, $C_{22}H_8$, and $C_{22}H_{10}$, respectively). These correspond the loss of C_2H_2 (or H_2+C_2) from the partly dehydrogenated DBPah structures $C_{24}H_8$, $C_{24}H_{10}$, and $C_{24}H_{12}$, respectively, which mimics the fragmentation behavior observed in DBPae. This pattern is then followed by signals at 246 and 248 amu ($C_{20}H_6$ and $C_{20}H_8$ – losses of two C_2H_2/ H_2+C_2 units), and at 220 and 222 amu ($C_{18}H_4$ and $C_{18}H_6$ – losses of three C_2H_2/H_2+C_2 units). CH loss still occurs, but it is more prominent after the loss of one or two C_2H_2 units. This shows itself as the CH losses occur simultaneously to the losses of one and two C_2H_2 units, rather than only showing up at larger irradiation doses than in DBPae. At this point it should be

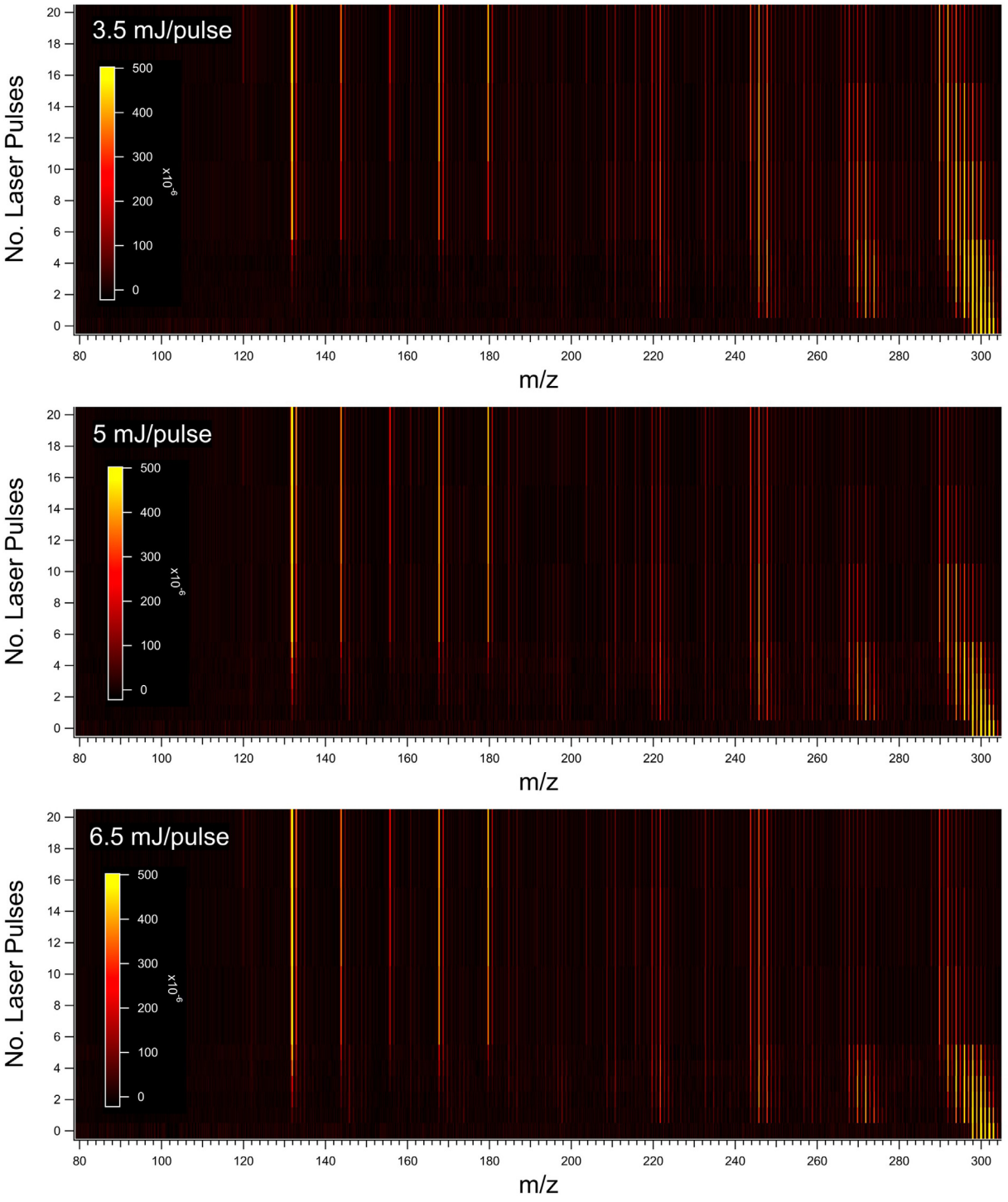

Fig. 4. Two-dimensional TOF-MS representation of the laser-induced photofragmentation of DBPah cation.

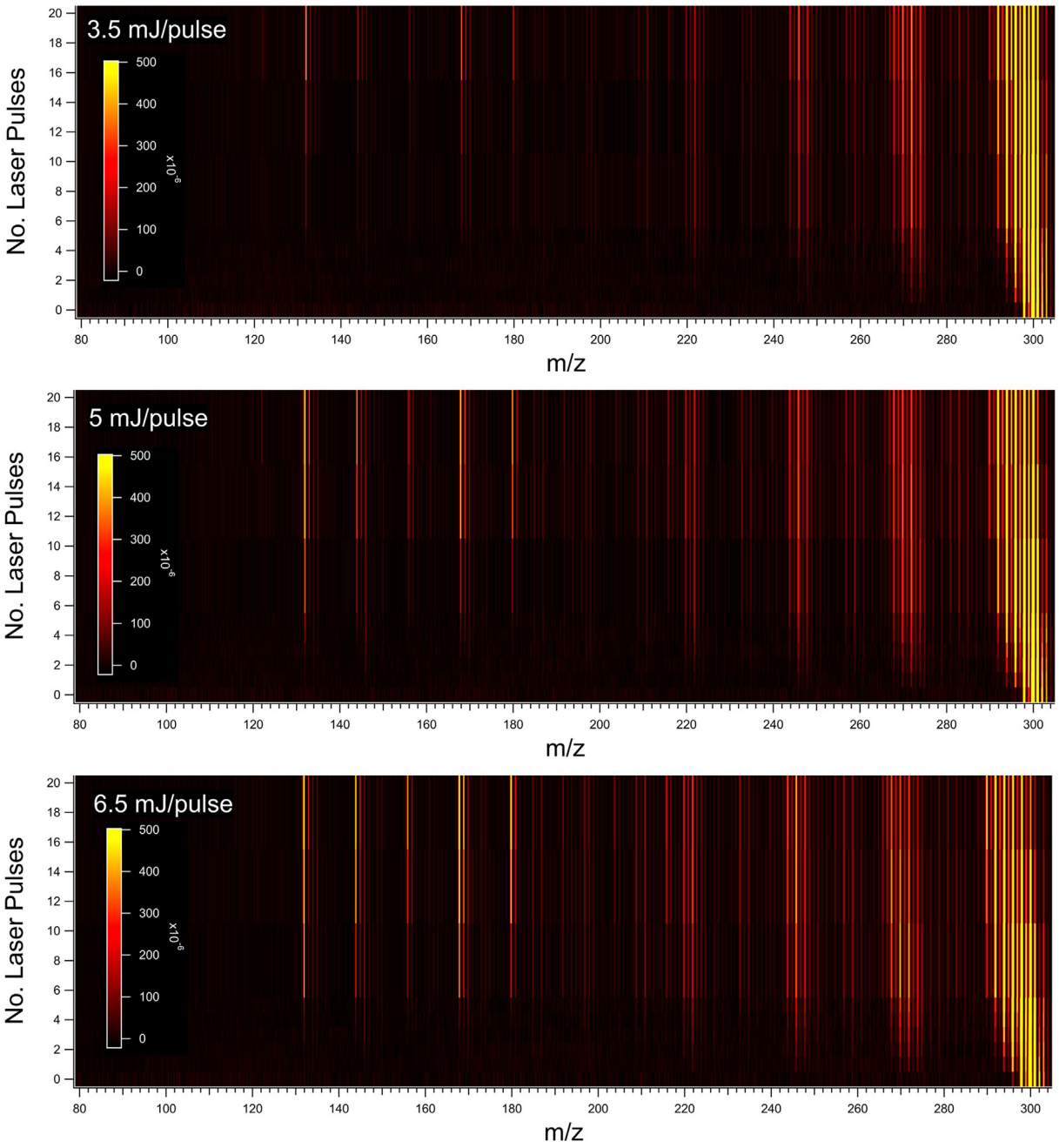

Fig. 5. Two-dimensional TOF-MS representation of the laser-induced photofragmentation of DBPal cation.

noted that it is impossible from this dataset to conclude whether a double C_2H_2 loss happens in two successive steps or a single step. The same goes for $CH + C_2H_2$ losses; they may occur in a single step where C_3H_5 (or even C_5H_5) breaks off the parent PAH.

When we inspect the middle and bottom panels of Fig. 4 we see two important trails of the fragmentation pattern. (i) The increased laser energy appears to have limited influence on the branching ratios of the C_{11}^+, C_{12}^+, C_{13}^+, C_{14}^+ and C_{15}^+ clusters. This will be discussed in more detail in section 3.4.1. (ii) The $C_{20}H_x$ (x = 4, 6, 8) fragments are still present even when using 6.5 mJ/pulse and twenty laser pulses. This is the same observation as before for DBPae where these fragments seemed to persist as they are probably both continually replenished by larger species fragmenting, as well as depleted and acting as important intermediates to other more stable fragmentation products. However, there should be a limit for these species acting as intermediates. If all of the parent in the trap is converted to smaller fragments, one would assume that eventually these species will become depleted in the trap as well.

Besides the $C_{20}H_x$ (x = 4, 6, 8) fragments, there are also the $C_{18}H_4$ and $C_{18}H_6$ fragments (220 and 222 amu, respectively) that seem to be still present in the 6.5 mJ/pulse experiments. Re-inspecting the bottom panel of Fig. 4 the case can be made that the $C_{18}H_6$ fragment is still present in the highest irradiation experiment and we can assume that this fragment could also be of some importance as an intermediate prior to further breakdown.

3.1.3. Dibenzo[a,l]pyrene (DBPal)

Fig. 5 presents the same TOF-MS matrix of DBPal as was presented for DBPae and DBPah in Figs. 3 and 4, respectively. In our dataset, DBPal is a bit special as the harsh electron impact

ionization depletes the parent to such an extent the DBPal-H_2 mass peaks exceeds the DBPal parent peak. This is, however, a reasonable starting point for further dissociation as $2H/H_2$ loss is the first observed fragmentation channel that is accessed in DBPal with low energy thresholds [44]. Hence, it can be envisioned that the first primary fragmentation step is mostly overcome with the electron impact ionization.

As in these two cases, the DBPal isomer does not completely dehydrogenate and the largest degree of dehydrogenation is observed to be $C_{24}H_2$ (290 amu). Likewise, as in DBPae and DBPah, the losses of C_2H_2 are significantly more dominant than the loss of CH and the molecule seems to favor subsequent losses of C_2H_2 although we do see the loss of CH, particularly around 258 and 260 amu ($C_{21}H_6$ and $C_{21}H_8$, respectively) and then followed by C_2H_2 loss at 232 and 234 amu ($C_{19}H_4$ and $C_{19}H_6$, respectively) but these are inferior to the principal C_2H_2 loss channels.

As in DBPah, the C_{11}^+, C_{12}^+, C_{13}^+, C_{14}^+ and C_{15}^+ carbon clusters are already observable at the lowest irradiation doses for 3.5 mJ/pulse (top panel of Fig. 5). These masses grow in significantly as the number of laser pulses increases. Interestingly, the even numbered clusters C_{12}^+ and C_{14}^+ seem to be clearly accompanied by signals corresponding to $C_{12}H_2^+$ and $C_{14}H_2^+$ while all the carbon clusters seem have residual C_nH^+ signals. However, the bare carbon clusters seem to only increase in intensity whereas the hydrogenated signals are quickly destroyed.

An important thing to note is that the partly dehydrogenated species seem to still be photo-resistant at high laser fluence. There are still plenty of fragmentation products but the parent and partly dehydrogenated parent species are not depleted at a level even distinctly close as found for DBPae and DBPah. In the case of all three laser pulse energies presented in Fig. 5, the DBPal parent (302 amu) becomes depleted before 20 laser pulses are sent into the ion trap.

It is only after this first loss of H_2 that the carbon PAH skeleton exhibits this aforementioned photo-resistivity unlike the other two isomers, DBPae and DBPah. Indeed, Rodriguez Castillo et al. found that DBPal loses two H atoms to form a stable more compact PAH with a pentagon forming in the bay region where the two H atoms are lost (see Fig. 5 in Ref. [44]). This results in the formation of Fluoreno [1,2,3,4,5,-b,c,d,e]pyrene which appears to be more resistive to fragmentation in our experiment, giving rise to the resistivity of H_2-losses observed in Fig. 5.

An important distinction from the other two DBP isomers that 20 pulses with 6.5 mJ/pulse did not entirely deplete the parent species as they were still prominent fragments in the ion trap after 20 pulses. Hence, to ensure that these results are comparable in terms of parent depletion, we recorded an additional pulse train for DBPal at 6.5 mJ/pulse but with the number of laser pulses between 10 and 70. The TOF-MS matrix of this additional pulse train is presented in Fig. 6.

From Fig. 6 we see that as the entire parent species is depleted, there are interesting differences that arise in the intensity of the different carbon clusters. Namely, the C_n^+ (n = 11–15) carbon clusters appear to be formed in quite similar ratios as before, with the main difference being a slightly enhanced formation of C_{14}^+ and C_{15}^+. For DBPae and DBPah, the formation of C_{11}^+ is clearly favored as the parent becomes depleted, but here the ratios between the three isomers are quite similar. The branching ratios between the carbon clusters C_n^+ ($n = 11$–15) will be up for discussion in the next section.

3.1.4. Carbon clusters, C_n^+ (n = 11–15)

A remarkable and consistent observation is that upon excitation all three DBPs result in the formation of pure carbon clusters, with $11 - 15$ carbon atoms. Normalized mass peaks for these C_n^+ clusters ($n = 11$–15) are all presented in Fig. 7. These were obtained from the mass spectra presented in the TOF-MS matrices in Figs. 3–5 and normalized according to the procedure described in section 2.2. Note that the vertical scales for a) to e) are all different.

Out of the five carbon clusters presented in Fig. 7, C_{11}^+ yields the strongest signals by far whereas the C_{12}^+, C_{13}^+, C_{14}^+, and C_{15}^+ mass signals seem to follow very similar formation trends among the three isomers. For DBPal, the formation of all of them is continually increasing and appears to start rising above the yields reached for the DBPae and DBPah isomers. Meanwhile, for DBPah, their formation seems to be decelerating with more laser pulses, reaching a plateau, and for DBPae, their yield is starting to decrease.

As the normalized peak areas can be deceptive to analyze we also present the branching ratios of the corresponding carbon clusters in Fig. 8. The branching ratios are calculated by dividing the peak area of a corresponding fragment with the combined peak areas of all the carbon cluster peaks in this analysis. I.e.

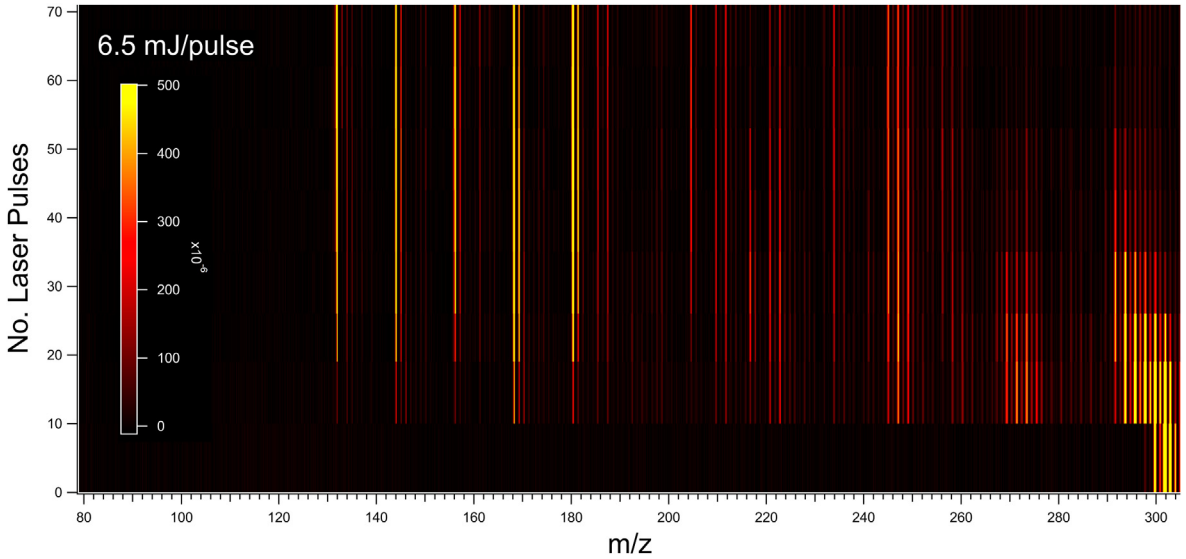

Fig. 6. Two-dimensional TOF-MS representation of the laser-induced photofragmentation of DBPal from the number of laser pulses being 10–70 with the length of each measurement cycle being 10 s.

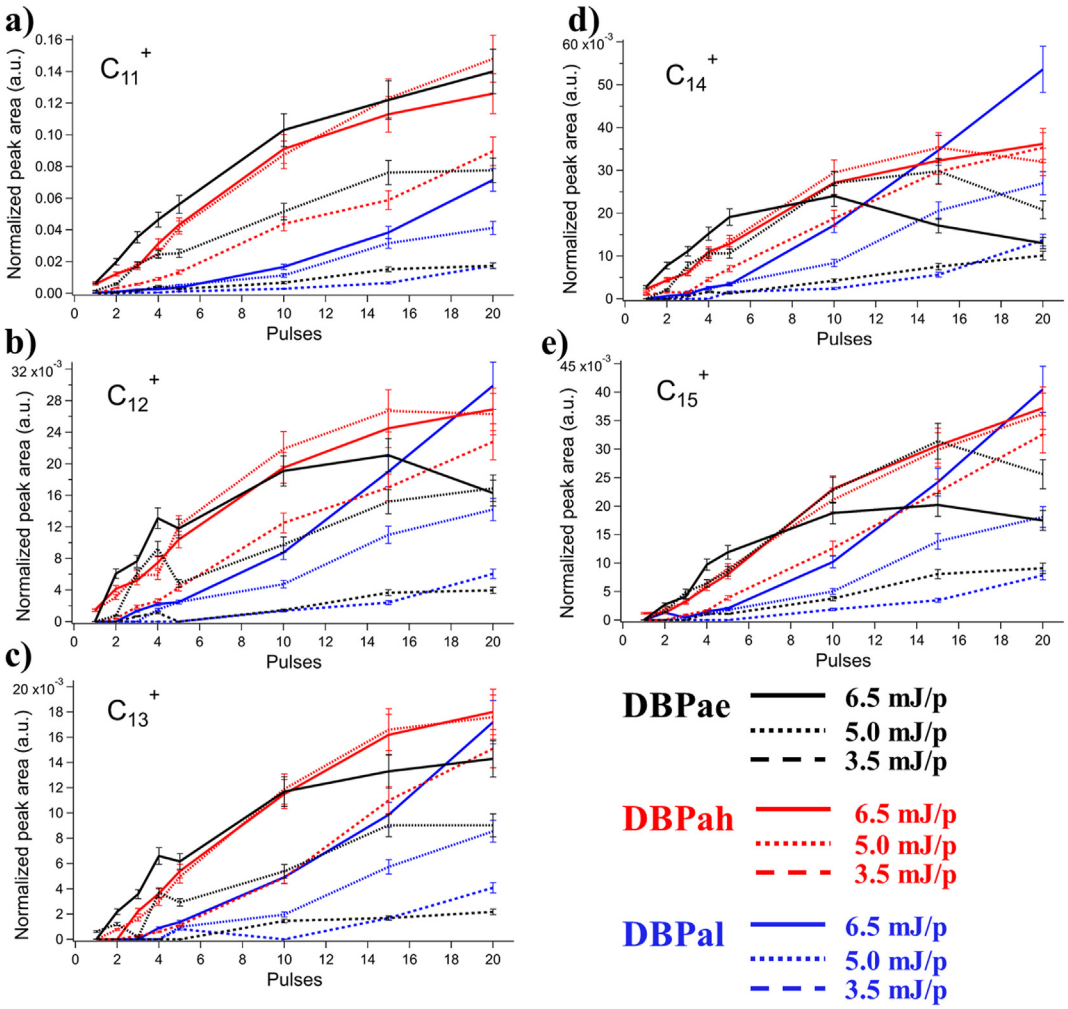

Fig. 7. Normalized mass peak areas corresponding to the most prevalent carbon clusters formed in the fragmentation of the three DBP isomers. Black traces correspond to DBPae, red traces to DBPah, and blue traces to DBPal. Solid lines trace mass signals recorded with 6.5 mJ per laser pulse, dotted lines 5.0 mJ/pulse, and dashed lines 3.5 mJ/pulse. Panels a) – e) show the mass signals pertaining to $C_{11}^{+} - C_{15}^{+}$.

$$BR_{C_n^+} = \frac{A_{C_n^+}}{\sum_{n=11}^{15} A_{C_n^+}}$$

For this discussion we only calculate the branching ratios starting at four laser pulses because that is where the collective mass signals for the carbon clusters become significant. When the branching ratios among the carbon clusters are inspected, the most prominent signal is that of the C_{11}^{+} mass fragment. In the case of all three isomers, the C_{11}^{+} signal dominates the mass spectra, but while it peaks around 50–60% for DBPae and DBPah, it plateaus around 35–40% for DBPal as, for this isomer, the branching ratios for the C_n^{+} ($n = 12–15$) clusters are on average higher as compared to DBPae and DBPah. This is consistent with what can be seen in the normalized peak areas in Fig. 7. This could be an indication of the nuanced roles that molecular structures play in the fragmentation process. If the first fragmentation step of DBPal is the loss of H_2 to form a planar (and more compact) fluorenopyrene, then that starting structure would appear to make the formation of the larger carbon clusters more facile.

The branching ratios also reveal some more subtle differences amongst the C_n^{+} ($n = 12–15$) carbon clusters. Namely, the C_{12}^{+} and C_{13}^{+} cluster branching ratios seem to plateau around similar and consistent values (between 5 and 15%), but the C_{14}^{+} and C_{15}^{+} show a larger spread in the branching ratios for larger radiation doses (between 5 and 30%). The largest differences are seen between DBPae and DBPal. It is becoming readily apparent that the C_{14}^{+} and C_{15}^{+} cluster yields are decreasing in DBPae but increasing in DBPal. The C_{12}^{+} and C_{13}^{+} signals, however, just appear to be plateauing.

All in all, what these results show, is that there is a large degree of similarity in the product yields of these carbon clusters for the three isomers studied here hinting at a universal PAH fragmentation mechanism that is (in part) irrespective of molecular structure, at least for the DBP species presented here, but with enough subtle and important nuances in the fragmentation behavior that each of these molecules needs to be treated separately to understand the link between molecular structure and ultimate fragmentation products.

3.1.5. *DBPal - laser exposure*

To ensure that the same level of fragmentation of DBPal was reached, an additional laser pulse train was recorded up to 70 pulses whose results are presented in Fig. 6. The total measurement cycle for this additional pulse train was 10 s whereas for all other pulse trains the measurement cycle was 5 s. The integrated masses and the branching ratios of corresponding to the 6.5 mJ/pulse trains of DBPal are presented in Fig. 9.

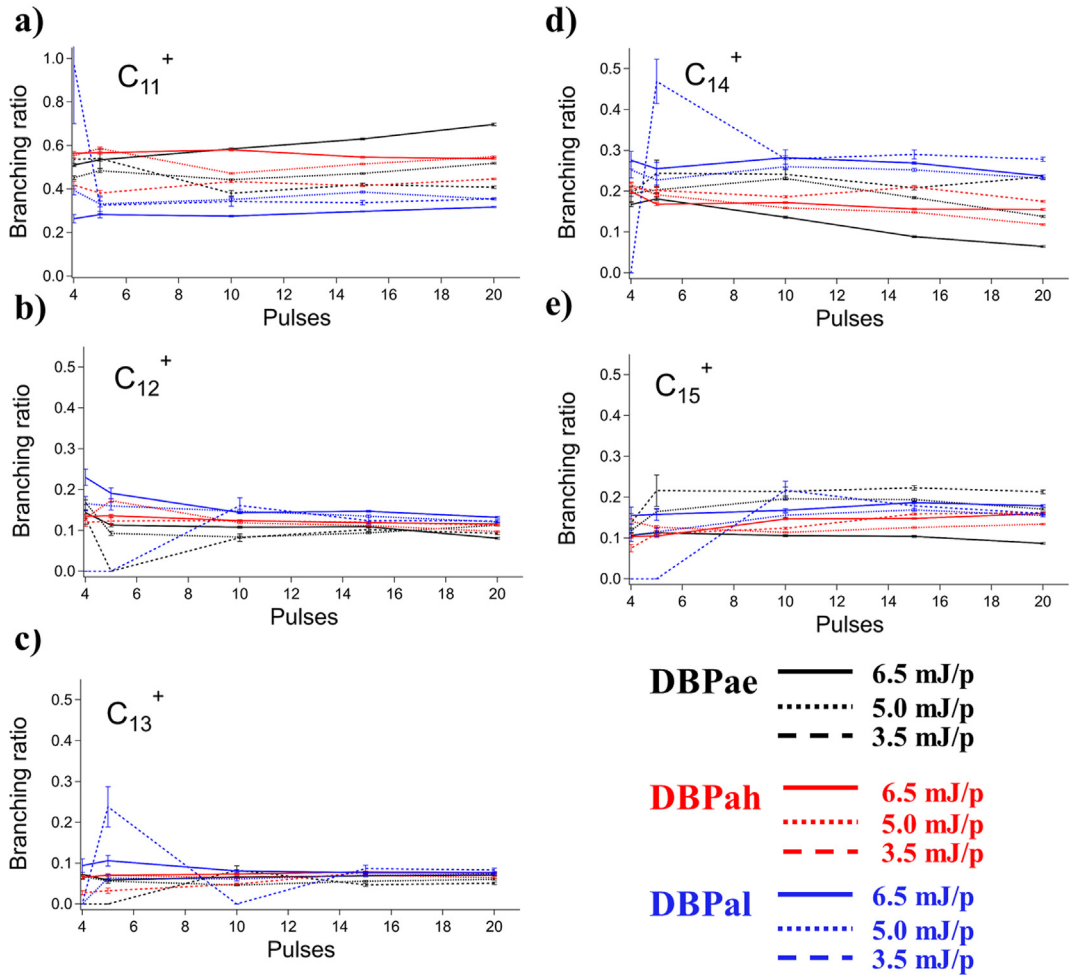

Fig. 8. Branching ratios corresponding to the most prevalent carbon clusters formed in the fragmentation of the three DBP isomers. All traces presented are consistent with those described in the caption of Fig. 7.

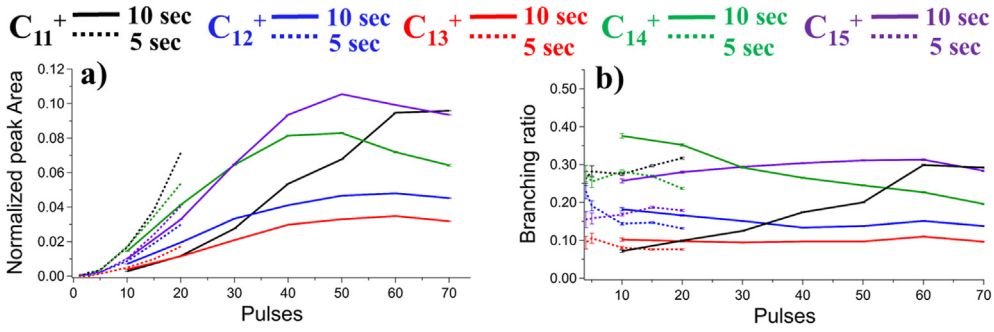

Fig. 9. Normalized mass peak areas (left panel) and branching ratios (right panel) corresponding to the $C_{11}^+ - C_{15}^+$ carbon clusters formed in the fragmentation of DBPal for the 5 s and 10 s cycle pulse trains.

There are a couple of stark differences in the mass peak areas and the branching ratios for the two pulse trains. An important thing to note is that in the longer measurement cycle for 20 laser pulses, the carbon cluster yield is always lower as compared to the shorter measurement cycle. After 20 laser pulses in the longer measurement cycle, there are still 5 s until the ions pass through to the reflectron TOF mass spectrometer. In comparison, within the shorter measurement cycle, the ions are ejected into the TOF-MS a few milliseconds after the twentieth laser pulse has passed through the ion trap.

There are a few ways that ions can deplete under these circumstances. The first is depletion due to collisions inside the trap with background gases. This means that ions can be depleted via collisions with other species in the trap but it is also possible that the RF voltage used for the ion trap becomes worse at holding on to the ions within the mass range as they may be at the cusp of the stability region of the ion trap. This effect is, however, very difficult to quantify and would require further experiments at lower RF voltages to fully explore the low-mass range below C_{11}^+ in order to observe the impact (if any) on the C_n^+ carbon cluster products.

Table 1
Summary of the number of laser pulses required to observe relevant fragmentation channels open up.

	DBPae	DBPah	DBPal
Complete H-loss	3.5 mJ/p: 3–4 pulses	3.5 mJ/p: 4–5 pulses	3.5 mJ/p: 5–10 pulses
	5.0 mJ/p: 3–4 pulses	5.0 mJ/p: 4–5 pulses	5.0 mJ/p: 5–10 pulses
	6.5 mJ/p: 3–4 pulses	6.5 mJ/p: 3–4 pulses	6.5 mJ/p: 5–10 pulses
1 x C_2H_2 loss	3.5 mJ/p: 1 pulse	3.5 mJ/p: 1 pulse	3.5 mJ/p: 1 pulse
	5.0 mJ/p: 1 pulse	5.0 mJ/p: 1 pulse	5.0 mJ/p: 1 pulse
	6.5 mJ/p: 1 pulse	6.5 mJ/p: 1 pulse	6.5 mJ/p: 1 pulse
2 x C_2H_2 loss	3.5 mJ/p: 1 pulse	3.5 mJ/p: 1 pulse	3.5 mJ/p: 4 pulses
	5.0 mJ/p: 1 pulse	5.0 mJ/p: 1 pulse	5.0 mJ/p: 2 pulses
	6.5 mJ/p: 1 pulse	6.5 mJ/p: 1 pulse	6.5 mJ/p: 1 pulse
3 x C_2H_2 loss	3.5 mJ/p: 2–3 pulses	3.5 mJ/p: 1 pulse	3.5 mJ/p: 4 pulses
	5.0 mJ/p: 2–3 pulses	5.0 mJ/p: 1 pulse	5.0 mJ/p: 2 pulses
	6.5 mJ/p: 1 pulse	6.5 mJ/p: 1 pulse	6.5 mJ/p: 2 pulses
1 x CH loss	3.5 mJ/p: 3–4 pulses	3.5 mJ/p: 3–4 pulses	3.5 mJ/p: 5 pulses
	5.0 mJ/p: 3–4 pulses	5.0 mJ/p: 3–4 pulses	5.0 mJ/p: 5 pulses
	6.5 mJ/p: not obs.	6.5 mJ/p: 3–4 pulses	6.5 mJ/p: 5 pulses
C_n^+	3.5 mJ/p: 5 pulses	3.5 mJ/p: 2 pulses	3.5 mJ/p: 5 pulses
	5.0 mJ/p: 3 pulses	5.0 mJ/p: 1 pulse	5.0 mJ/p: 3 pulses
	6.5 mJ/p: 2 pulses	6.5 mJ/p: 1 pulse	6.5 mJ/p: 3 pulses

There is an interesting trend we see in the longer measurement cycle which was perhaps hinted at in the results described in the previous section. Between 50 and 70 pulses, the C_{14}^+ and C_{15}^+ masses are depleted whilst the C_{11}^+ peak signal keeps growing. In fact, this depletion is so significant that C_{11}^+ becomes the co-dominant signals along with C_{15}^+. A similar trend is observed in Fig. 7 for DBPae where the C_{14}^+ and C_{15}^+ signals continued to deplete at higher radiation doses while the C_{11}^+ mass signal kept increasing. Hence, the longer measurement cycle of DBPal could be hinting at a similar fragmentation mechanism as that of DBPae, *i.e.* that C_{11}^+ isomers could be forming from C_{14}^+ and C_{15}^+ by losing C_3 or C_4 units. Similar decreases in the C_{12}^+ and C_{13}^+ mass signals are also observed but no solid conclusions on this point can be drawn. Even though the decrease in the C_{12}^+-C_{15}^+ signals correlate with the increase in the C_{11}^+ signal, that is not indication of a causal relationship. Rather, to fully reveal the extent of the mechanisms of these fragmentations and exploring the potential energy surface is out of scope of this paper, but possible mechanisms will be discussed in the next section.

4. Discussion

4.1. PAH fragmentation

Characterizing the difference in the molecular geometry of PAHs is often done by considering the number of solo, duo, trio, and quarto hydrogen atoms, as well as so-called bay and non-bay hydrogen atoms [52]. Table 2 shows how the DBP isomers in this work, along with fluorenopyrene isomer that forms upon 2H/H_2-loss from DBPal [44], differ in terms of these geometrical classifications. Irregular PAHs (such as the DBP isomers considered here) usually contain various numbers of solo, duo, trio, and quarto hydrogens but more compact PAHs tend to contain only solo and duo H atoms [52]. In the case of the fluorenopyrene isomer, it contains no quarto hydrogen atoms but nine trio hydrogen atoms which clearly differentiates it from the other DBP isomers.

Table 2
Numbers of solo, duo, trio, quarto, bay, and non-bay hydrogen atoms in the three DBP isomers and the fluorenopyrene isomer that can form from H_2-loss from DBPal.

	DBPae	DBPah	DBPal	Fluorenopyrene
Solo H atoms	1	2	1	1
Duo H atoms	2	4	2	2
Trio H atoms	3	0	3	9
Quarto H atoms	8	8	8	0
Bay H atoms	6	4	4	4
Non-Bay H atoms	8	10	10	8

A fair body of work exists on the fragmentation patterns and fragmentation dynamics of PAHs. Jochims et al. [33,36] showed that the lowest energy fragmentation pathways from PAHs are the loss of hydrogen(s) and the loss of C_2H_2. The three DBP isomers in this work appear to follow the same trend as the loss of a single CH/CH_3-moiety from the parent species appears as a minor product at higher laser pulses than is required to lose H_2 and/or C_2/C_2H_2 units (see Table 1). Other higher energy channels were expected to involve C_3H_3 and C_2H but these have not been observed experimentally and it is not possible to decipher from our experiments whether losses of CH are followed by C_2/C_2H_2 losses, vice versa, or whether these losses occur as a single step (i.e. C_3H/C_3H_3).

Ekern et al. [34] also showed that fragmentation of PAHs of varying sizes and symmetry can be categorized as H-loss only, H- & C-loss, and "completely photodestroyed". Although this classification is quite vague, there are some important things to note. Among the most important is that the loss of C_2H_2 is facilitated by the presence of at least one "exposed" aromatic ring, *i.e.*, containing a quarto of hydrogen atoms. Nonetheless, this comes with some exceptions among the PAHs studied therein, namely triphenylene, and fluorene. Linking this observation to our results, it does indeed appear to help C_2/C_2H_2 losses to have two exposed aromatic rings (like the DBP isomers have). But it is also interesting that it appears that the fluorenopyrene isomer seems not to inhibit C_2/C_2H_2 loss.

Ekern et al. [34] observed that the coronene cation and the naphtho [2,3-a]pyrene cation lose all their hydrogen atoms upon photolysis to give the common end product C_{24}^+. This led to speculation about common intermediates formed by ring opening and isomerization. There has been evidence observed in the past as well that there is a preference for dissociation via certain pathways and this preference arises from common reaction mechanisms that produce the same fragment product ions [29]. But in the case of the DBP isomers and fluorenopyrene, none of these molecules seem to prefer complete dehydrogenation. As a majority of the H atoms in all of these structures are either quartos in exposed aromatic rings in the DBPs or trios on fluorenopyrene, this seems to be the major hurdle in completely losing all of the H atoms prior to losing members of the carbon skeletons of the PAHs.

Regarding larger PAHs as previously studied with the i-POP apparatus, it was shown that the pericondensed HBC cation ($C_{42}H_{18}^+$) preferably loses its H-atoms, revealing a bare carbon ("graphene like") skeleton that subsequently undergoes C_2 losses

up until C_{32}^+ [53]. Similar to HBC, the planar PAHs $C_{60}H_{22}$ and $C_{66}H_{26}$ undergo complete dehydrogenation before subsequently losing C_2 units [21]. After the formation of C_{32}^+, the losses of C_2 seemed to come to a grinding halt and dominating the mass spectra were the signals of C_n^+ (n = 17–20) carbon clusters. Possibly also smaller clusters formed, but Zhen et al. did not increase the laser fluence enough, or set the RF voltage on the ion trap low enough, to observe the formation of any smaller carbon clusters. Repeating these measurements of larger PAHs would be of great interest to reveal whether the C_n^+ (n = 11–15) carbon clusters form as well and if they form in similar branching ratios as observed in this work for the DBP isomers.

Recently, Pla et al. [54], performed a detailed inspection of the structural diversity of $C_{24}H_n$ (n = 0, 6, 12, 18, 24) clusters in their potential energy surfaces up to 20–25 eV. There are several notable results of theirs that are directly relevant to our work. In accordance with general structural optimizations, carbon cluster structures can be divided into cages, flakes, pretzels and branched structures (see Fig. 2 in Pla et al. [54]). These categories can be identified by the number of sp^2 hydridized carbon atoms in the structure (so-called asphericity parameter) and the number of pentagons and hexagons in the structure [54]. Regarding the structures that are most relevant to our work (namely C_{24}, $C_{24}H_6$ and $C_{24}H_{12}$), the most stable configurations are found to be flakes, pretzels and branched structures as practically no caged structures were found to be relevant unlike that of C_{60} carbon clusters [55,56]. Pla et al. discussed the presence of rings in the molecular structures in the calculations and find that above 15 eV, the appearance of heptagons in the $C_{24}H_{12}$ isomers become more common than hexagons. They did not look into formation of rings containing more than eight carbon atoms. Considering such starting points, it is fairly easy to see how carbon clusters comprising 11 to 15 atoms can be separated from branched structures, pretzels, and flakes (see Fig. 2 in Ref. [54]). Pla et al. found that upon fragmentation, C_{24} carbon clusters have an affinity to form carbon clusters with twelve carbon atoms or thereabout. Our results indicating the importance of C_n^+ (n = 11–15) carbon clusters seem to go very well with this observation. It would be of interest to inspect the formation of rings from cationic hydrocarbon clusters to inspect if a positive charge could be instrumental in building carbon rings comprising more than eight carbon atoms.

The formation of carbon clusters such as those observed in this work has also been explored with regard to the dissociation of the pyrene cation as discussed by West et al. [57]. They suggested a pathway forming a cyclic C_{14}^+ isomer starting from the pyrene cation ($C_{16}H_{10}^+$) where the aromatic C–C bonds in the carbon skeleton start breaking apart after the ion partly dehydrogenizes before forming a cyclo [14]carbon that initially retains 1–3 H atoms that are sequentially lost upon further excitation. This scenario also fits our results exceedingly well as many of the C_n^+ (n = 11–15) clusters are initially accompanied by two H atoms which are subsequently lost when the number of laser pulses are increased.

Recent work by Trinquier et al. [58] also showed that breaking aromatic bonds in coronene- and pyrene-type PAHs to start forming pretzels and flakes, requires energies between 5 and 10 eV to surpass the appropriate barriers. When our results are combined with the previous findings of Pla et al. [54], Trinquier et al. [58], and West et al. [57], a picture seems to emerge where a large number of intermediates are potentially formed where (i) the molecule may become partly dehydrogenated, (ii) C_2H_2 units dissociate easily from the molecule, (iii) aromatic C–C bonds in the PAH skeleton are broken or rearranged to accommodate heptagons, and (iv) carbon clusters break off as rings or other structures that may undergo molecular rearrangements that retain the positive charge from the PAH cation, sometimes with a few H atoms that (v) subsequently break off the carbon rings. An example of one such scenario is visualized in Fig. 10.

Another interesting facet to PAH fragmentation that we observe in this work is the apparent competition between statistical (e.g., H_2-, C_2H_2-losses) and non-statistical (e.g., CH-losses) fragmentation processes. Despite PAHs have large heat capacities they will eventually fragment unless there are sufficiently fast competing (radiative) cooling processes [59]. The fragmentations in our experiments are induced by multi-photon excitations and as such, those processes can be highly nonlinear where different numbers of photons can grant access to a myriad of different fragmentation pathways, some via electronically excited states. Statistical fragmentation processes imply that the energy donated to the system is equally distributed over the molecules' degrees of freedom before it fragments. For the most part we observe statistical fragmentation processes to dominate (i.e., C_2H_2-losses are more prevalent than CH-losses), but the fact that we observe clear CH-losses and a competition with C_2H_2-losses could mean that there is inhomogeneity in how the laser pulse hits the ion cloud in the experiment (i.e., some molecules absorbing a greater number of photons than others, on average). However, without detailed calculations of the potential energy surface, it is entirely speculative whether this affects the outcomes of fragmentation in our experiment. Such calculations have been performed for the fragmentation of the pyrene cation when it is impacted by high energetic protons [60], but such a calculation is outside the scope of this paper.

4.2. Astrophysical significance

Assuming the GRANDPAH hypothesis holds true, then there are a lot of different smaller PAHs that are photodestroyed by UV photons, collisions etc. Our results and that of recent studies by other groups seem to indicate that PAHs outside of the GRANDPAH family, favor

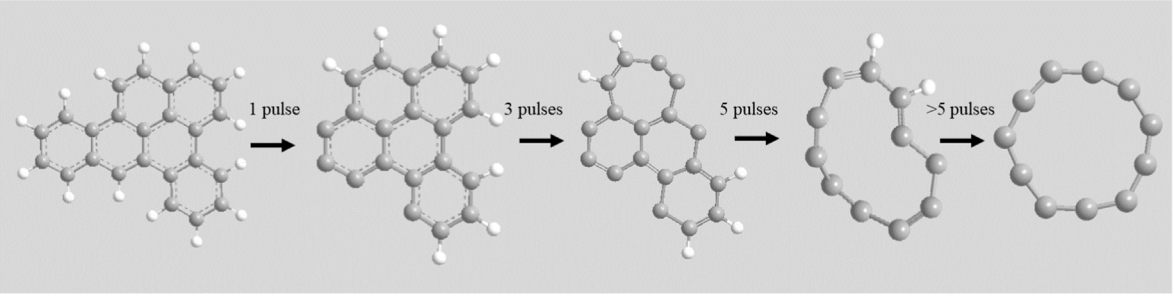

Fig. 10. An imagining of a potential pathway to form the C_{11}^+ carbon cluster from DBPae based on our results (using 3.5 mJ/pulse) and the theoretical work of Pla et al. [54], Trinquier et al. [58] and West et al. [57]. The first two steps require the apparently facile elimination of first two C_2H_2 units (1 pulse) and then a third C_2H_2 unit with the rupture of a couple of aromatic bonds and the formation of a heptagon (3 pulses). From there a $C_{11}H_x^+$ unit could break off the parent with a few H atoms (5 pulses) which are subsequently dissociated to reveal a single C_{11}^+ unit (>5 pulses). The structures were optimized with the chemistry visualization software Chem3D.

universal fragmentation pathways that eventually produce C_n^+ ($n = 11–15$) carbon clusters. On the exact mechanism by which they form we can theorize that partly dehydrogenated PAHs in the form of pretzels or flakes, lose an ionized carbon cluster. For branched structures, however, it is perhaps more likely that linear carbon chains dissociate. Smaller PAHs have also been observe to form smaller carbon clusters C_n^+ (n = 2–13) by absorbing X-ray photons (hν = 275, 310 & 2500 eV) in a top-down chemical paradigm, however, it may be more likely that their formation proceeds via Coulomb-explosions rather than sequential C/H losses [61]. This is also interesting considering that no such carbon clusters were observed to form from X-ray absorption of coronene cations between 283 and 305 eV [62]. This is perhaps indicative of there being even more nuances in fragmentation patterns expected in more compact PAHs in the X-ray regime, like coronene, as opposed to smaller less compact ones studied by Monfredini et al. [61].

This also brings about questions concerning the photon wavelengths used in this work and how that could influence the branching ratios of the carbon clusters formed. Previous work by Joblin [63] showed that carbon clusters C_n^+ (n = 10–21) could form in different branching ratios from our work (with C_{14}^+ being the most abundant), by irradiating the coronene cation by a Xe arc lamp and 480 nm photons. Investigating further the wavelength dependence of fragmentation products is clearly of future interest to further elucidate the fragmentation mechanisms involved and their energetics.

The suggestion that larger carbon cages such as C_{44}, C_{50} and C_{56} are carriers of the DIBs has been discussed before but without conclusive assignment to any astronomical features [64]. Considering the ongoing work dedicated to exploring the connections between carbon clusters and the DIBs [65–67], then the apparent importance of the C_n^+ ($n = 11–15$) carbon clusters needs to be further examined in terms of their optical spectra. Recently, optical spectra of even-numbered cyclo[n]carbons complexes with N_2 were recorded with action spectroscopy [68] and preliminary analysis appears to indicate that there may be matches with DIBs for C_{10}^+ and/or C_{14}^+, but at present it is unknown to what extent the spectra are shifted because of the complex with N_2, which makes direct comparisons with known DIBs more difficult. This study shows that these species may arise as breakdown products of PAHs, perhaps with non-linear geometries. The optical spectra of linear carbon species up to C_{21} have been measured [69,70], but these have been theorized to form in a bottom up process as these molecules can be created in a plasma discharge using e.g. acetylene (C_2H_2) as a precursor. However, our results indicate that a top-down mechanism starting from smaller PAHs that should not survive the harsh radiation fields in various interstellar regions, could be collectively playing an important role in producing new non-linear molecular species.

5. Summary and conclusions

We have presented here the fragmentation patterns of three isomeric PAH cations, namely, dibenzo[a,e]pyrene, dibenzo[a,h]pyrene and dibenzo[a,l]pyrene. Through the complex fragmentations patterns wrought by laser-induced dissociation, a clear pattern of carbon cluster formation emerges. Regardless of symmetry of the parent PAH cation, the formation of C_n^+ ($n = 11–15$) carbon clusters proceeds in similar branching ratios between the three isomers studied. This is an interesting result that hints for favored fragmentation steps, but studying larger PAHs is required to verify that C_n^+ ($n = 11–15$) carbon clusters are formed from larger PAH species as well.

The main takeaway from this work is finding of a possible universal PAH fragmentation mechanism that could hold clues to the photochemistry of UV-rich regions in space and could imply that the C_n^+ ($n = 11–15$) carbon clusters consistently formed and retained in the ion trap despite continued laser irradiation might be appropriate candidates as carriers of the elusive DIBs. This may hold true especially for C_{11}^+ which appears very photo-resistant and has been observed in asteroid samples [71] and laboratory-grown interstellar dust analogs [72], but these carbon clusters could play a very important role for PAH-rich matter born out of reddened stars at the end of their lifetimes and ejected into the diffuse interstellar medium.

Author statement

H. R. Hrodmarsson: Data curation, Formal analysis, Investigation, Writing – original draft, Review & editing.

J. Bouwman: Methodology, Formal analysis, Investigation, Writing, Review & editing.

A. G. G. M. Tielens: Resources, Review & editing.

H. Linnartz: Project administration, Investigation, Review & editing.

Declaration of competing interest

The authors declare that they have no known competing financial interests or personal relationships that could have appeared to influence the work reported in this paper.

Acknowledgments

H. R. H. acknowledges funding from the European Union's Horizon 2020 research and innovation programme under grant agreement No. 838372. J. B. acknowledges the Netherlands Organisation for Scientific Research (Nederlandse Organisatie voor Wetenschappelijk Onderzoek, NWO) for a Vidi grant (grant number 723.016.006) which supported this work. Studies of interstellar PAHs at Leiden Observatory are supported through a Spinoza award. This work was supported in part by NASA's Solar System Exploration Research Virtual Institute (SSERVI): Institute for Modeling Plasma, Atmosphere, and Cosmic Dust (IMPACT).

References

[1] A.G.G.M. Tielens, Interstellar polycyclic aromatic hydrocarbon molecules, Annu. Rev. Astron. Astrophys. 46 (2008) 289–337, https://doi.org/10.1146/annurev.astro.46.060407.145211.

[2] I. Cherchneff, The formation of polycyclic aromatic hydrocarbons in evolved circumstellar environments. https://doi.org/10.1051/eas/1146019, 2011.

[3] J. Cernicharo, M. Agúndez, C. Cabezas, B. Tercero, N. Marcelino, J.R. Pardo, P. de Vicente, Pure hydrocarbon cycles in TMC-1: discovery of ethynyl cyclopropenylidene, cyclopentadiene, and indene, A&A 649 (2021) L15, https://doi.org/10.1051/0004-6361/202141156.

[4] A.M. Burkhardt, K.L.K. Lee, P.B. Changala, C.N. Shingledecker, I.R. Cooke, R.A. Loomis, H. Wei, S.B. Charnley, E. Herbst, M.C. McCarthy, B.A. McGuire, Discovery of the pure polycyclic aromatic hydrocarbon indene (c-C_9H_8) with GOTHAM observations of TMC-1, ApJL 913 (2021) L18, https://doi.org/10.3847/2041-8213/abfd3a.

[5] B.A. McGuire, R.A. Loomis, A.M. Burkhardt, K.L.K. Lee, C.N. Shingledecker, S.B. Charnley, I.R. Cooke, M.A. Cordiner, E. Herbst, S. Kalenskii, M.A. Siebert, E.R. Willis, C. Xue, A.J. Remijan, M.C. McCarthy, Detection of two interstellar polycyclic aromatic hydrocarbons via spectral matched filtering, Science 371 (2021) 1265–1269, https://doi.org/10.1126/science.abb7535.

[6] G. Herbig, The diffuse interstellar bands, Annu. Rev. Astron. Astrophys. 33 (1995) 19–73, https://doi.org/10.1146/annurev.aa.33.090195.000315.

[7] P.J. Sarre, The diffuse interstellar bands: a major problem in astronomical spectroscopy, J. Mol. Spectrosc. 238 (2006) 1–10, https://doi.org/10.1016/j.jms.2006.03.009.

[8] N.L.J. Cox, J. Cami, L. Kaper, P. Ehrenfreund, B.H. Foing, B.B. Ochsendorf, S.H.M. van Hooff, F. Salama, VLT/X-Shooter survey of near-infrared diffuse interstellar bands, Astron. Astrophys. 569 (2014), https://doi.org/10.1051/0004-6361/201323061.

[9] F. Huisken, G. Rouillé, M. Steglich, Y. Carpentier, C. Jäger, T. Henning, Laboratory studies on the role of PAHs as DIB carriers, Proc. Int. Astron. Union 9 (2014), https://doi.org/10.1017/S1743921313015974.

[10] F. Salama, E.L. Bakes, L.J. Allamandola, A.G.G.M. Tielens, Assessment of the polycyclic aromatic hydrocarbon-diffuse interstellar band proposal, Astrophys. J. 458 (1996) 621–636, https://doi.org/10.1086/176844.
[11] A. Pathak, P. Sarre, Protonated PAHs as Carriers of Diffuse Interstellar Bands vol. 391, Monthly Notices of the Royal Astronomical Society: Letters, 2008, https://doi.org/10.1111/j.1745-3933.2008.00544.x. L10–L14.
[12] F. Salama, G.A. Galazutdinov, J. Krełowski, L. Biennier, Y. Beletsky, I.-O. Song, Polycyclic aromatic hydrocarbons and the diffuse interstellar bands, A Survey, ApJ. 728 (2011) 154, https://doi.org/10.1088/0004-637X/728/2/154.
[13] E.K. Campbell, M. Holz, D. Gerlich, J.P. Maier, Laboratory confirmation of C_{60}^+ as the carrier of two diffuse interstellar bands, Nature 523 (2015) 322+, https://doi.org/10.1038/nature14566.
[14] M. Kuhn, M. Renzler, J. Postler, S. Ralser, S. Spieler, M. Simpson, H. Linnartz, A.G.G.M. Tielens, J. Cami, A. Mauracher, Y. Wang, M. Alcami, F. Martin, M.K. Beyer, R. Wester, A. Lindinger, P. Scheier, Atomically resolved phase transition of fullerene cations solvated in helium droplets, Nat. Commun. 7 (2016), https://doi.org/10.1038/ncomms13550.
[15] M.A. Cordiner, H. Linnartz, N.L.J. Cox, J. Cami, F. Najarro, C.R. Proffitt, R. Lallement, P. Ehrenfreund, B.H. Foing, T.R. Gull, P.J. Sarre, S.B. Charnley, Confirming interstellar C_{60}^+ using the hubble space telescope, Astrophys. J. 875 (2019) L28, https://doi.org/10.3847/2041-8213/ab14e5.
[16] J. Cami, J. Bernard-Salas, E. Peeters, S.E. Malek, Detection of C_{60} and C_{70} in a young planetary nebula, Science 329 (2010) 1180–1182, https://doi.org/10.1126/science.1192035.
[17] K. Sellgren, M.W. Werner, J.G. Ingalls, J.D.T. Smith, T.M. Carleton, C. Joblin, C_{60} in reflection nebulae, Astrophys. J. Lett. 722 (2010), https://doi.org/10.1088/2041-8205/722/1/L54. L54–L57.
[18] K. Hansen, R. Richter, M. Alagia, S. Stranges, L. Schio, P. Salen, V. Yatsyna, R. Feifel, V. Zhaunerchyk, Single photon thermal ionization of C_{60}, Phys. Rev. Lett. 118 (2017), https://doi.org/10.1103/PhysRevLett.118.103001.
[19] O. Berné, J. Montillaud, C. Joblin, Top-down formation of fullerenes in the interstellar medium, A&A. 577 (2015) A133, https://doi.org/10.1051/0004-6361/201425338.
[20] O. Berné, A.G.G.M. Tielens, Formation of buckminsterfullerene (C_{60}) in interstellar space, Proc. Natl. Acad. Sci. U. S. A 109 (2012) 401–406, https://doi.org/10.1073/pnas.1114207108.
[21] J. Zhen, P. Castellanos, D.M. Paardekooper, H. Linnartz, A.G.G.M. Tielens, Laboratory formation of fullerenes from PAHS: top-down interstellar chemistry, Astrophys. J. Lett. 797 (2014), https://doi.org/10.1088/2041-8205/797/2/L30.
[22] P. Castellanos, O. Berné, Y. Sheffer, M.G. Wolfire, A.G.G.M. Tielens, C_{60} in photodissociation regions, Astrophys. J. 794 (2014), https://doi.org/10.1088/0004-637X/794/1/83.
[23] J. Bouwman, A.J. de Haas, J. Oomens, Spectroscopic evidence for the formation of pentalene$^+$ in the dissociative ionization of naphthalene, Chem. Commun. 52 (2016) 2636–2638, https://doi.org/10.1039/C5CC10090A.
[24] A.J. de Haas, J. Oomens, J. Bouwman, Facile pentagon formation in the dissociation of polyaromatics, Phys. Chem. Chem. Phys. 19 (2017) 2974–2980, https://doi.org/10.1039/C6CP08349H.
[25] M.N. McCabe, P. Hemberger, E. Reusch, A. Bodi, J. Bouwman, Off the beaten path: almost clean formation of indene from the *ortho*-benzyne + allyl reaction, J. Phys. Chem. Lett. 11 (8) (2020) 2859–2863, https://doi.org/10.1021/acs.jpclett.0c00374.
[26] H. Andrews, C. Boersma, M.W. Werner, J. Livingston, L.J. Allamandola, A.G.G.M. Tielens, PAH emission at the bright locations of PDRs: the grandPAH hypothesis, APJ (Acta Pathol. Jpn.) 807 (2015) 99, https://doi.org/10.1088/0004-637X/807/1/99.
[27] J. Bouwman, P. Castellanos, M. Bulak, J. Terwisscha van Scheltinga, J. Cami, H. Linnartz, A.G.G.M. Tielens, Effect of molecular structure on the infrared signatures of astronomically relevant PAHs, A&A 621 (2019) A80, https://doi.org/10.1051/0004-6361/201834130.
[28] J. Pety, D. Teyssier, D. Fossé, M. Gerin, E. Roueff, A. Abergel, E. Habart, J. Cernicharo, Are PAHs precursors of small hydrocarbons in photodissociation regions? The Horsehead case, A&A 435 (2005) 885–899, https://doi.org/10.1051/0004-6361:20041170.
[29] S.J. Pachuta, H.I. Kenttamaa, T.M. Sack, R.L. Cerny, K.B. Tomer, M.L. Gross, R.R. Pachuta, R.Graham Cooks, Excitation and dissociation of isolated ions derived from polycyclic aromatic hydrocarbons, J. Am. Chem. Soc. 110 (1988) 657–665, https://doi.org/10.1021/ja00211a001.
[30] C. Lifshitz, Energetics and dynamics through time-resolved measurements in mass spectrometry: aromatic hydrocarbons, polycyclic aromatic hydrocarbons and fullerenes, Int. Rev. Phys. Chem. 16 (1997) 113–139, https://doi.org/10.1080/014423597230235.
[31] Y. Ling, C. Lifshitz, Time-Dependent mass spectra and breakdown graphs. 21. $C_{14}H_{10}$ isomers, J. Phys. Chem. A. 102 (1998) 708–716, https://doi.org/10.1021/jp973167w.
[32] S. Panchagnula, J. Bouwman, D.B. Rap, P. Castellanos, A. Candian, C. Mackie, S. Banhatti, S. Brünken, H. Linnartz, A.G.G.M. Tielens, Structural investigation of doubly-dehydrogenated pyrene cations, Phys. Chem. Chem. Phys. 22 (2020) 21651–21663, https://doi.org/10.1039/D0CP02272A.
[33] H.W. Jochims, H. Baumgartel, S. Leach, Structure-dependent photostability of polycyclic aromatic hydrocarbon cations: laboratory studies and astrophysical implications, APJ (Acta Pathol. Jpn.) 512 (1999) 500–510, https://doi.org/10.1086/306752.
[34] S.P. Ekern, A.G. Marshall, J. Szczepanski, M. Vala, Photodissociation of gas-phase polycylic aromatic hydrocarbon cations, J. Phys. Chem. A. 102 (1998) 3498–3504, https://doi.org/10.1021/jp980488e.
[35] Bori Shushan, S.H. Safe, R.K. Boyd, Mass spectrometry of polycyclic aromatic hydrocarbons by linked-scan studies of metastable ions, Anal. Chem. 51 (1979) 156–158, https://doi.org/10.1021/ac50037a043.
[36] H. Jochims, E. Ruhl, H. Baumgartel, S. Tobita, S. Leach, Size effects on dissociation rates of polycyclic aromatic hydrocarbon cations - laboratory studies and astrophysical implications, Astrophys. J. 420 (1994) 307–317, https://doi.org/10.1086/173560.
[37] B. West, S. Rodriguez Castillo, A. Sit, S. Mohamad, B. Lowe, C. Joblin, A. Bodi, P.M. Mayer, Unimolecular reaction energies for polycyclic aromatic hydrocarbon ions, Phys. Chem. Chem. Phys. 20 (2018) 7195–7205, https://doi.org/10.1039/c7cp07369k.
[38] B. West, C. Joblin, V. Blanchet, A. Bodi, B. Sztáray, P.M. Mayer, On the dissociation of the naphthalene radical cation: new iPEPICO and tandem mass spectrometry results, J. Phys. Chem. A. 116 (2012) 10999–11007, https://doi.org/10.1021/jp3091705.
[39] B. West, L. Lesniak, P.M. Mayer, Why do large ionized polycyclic aromatic hydrocarbons not lose C_2H_2? J. Phys. Chem. A. 123 (2019) 3569–3574, https://doi.org/10.1021/acs.jpca.9b01879.
[40] B. West, A. Sit, A. Bodi, P. Hemberger, P.M. Mayer, Dissociative photoionization and threshold photoelectron spectra of polycyclic aromatic hydrocarbon fragments: an imaging photoelectron photoion coincidence (iPEPICO) study of four substituted benzene radical cations, J. Phys. Chem. A. 118 (2014) 11226–11234, https://doi.org/10.1021/jp5085982.
[41] P. Castellanos, A. Candian, J. Zhen, H. Linnartz, A.G.G.M. Tielens, Photoinduced polycyclic aromatic hydrocarbon dehydrogenation the competition between H- and H_2 -loss, A&A 616 (2018) A166, https://doi.org/10.1051/0004-6361/201833220.
[42] J. Bouwman, H. Linnartz, A.G.G.M. Tielens, Mid-infrared spectroscopic signatures of dibenzopyrene cations – the effect of symmetry on PAH IR spectroscopy, J. Mol. Spectrosc. 378 (2021) 111458, https://doi.org/10.1016/j.jms.2021.111458.
[43] J. Zhen, S.R. Castillo, C. Joblin, G. Mulas, H. Sabbah, A. Giuliani, L. Nahon, S. Martin, J.-P. Champeaux, P.M. Mayer, VUV photo-processing of PAH cations: quantitative study on the ionization versus fragmentation processes, Astrophys. J. 822 (2016) 113, https://doi.org/10.3847/0004-637X/822/2/113.
[44] S. Rodriguez Castillo, A. Simon, C. Joblin, Investigating the importance of edge-structure in the loss of H/H_2 of PAH cations: the case of dibenzopyrene isomers, Int. J. Mass Spectrom. 429 (2018) 189–197, https://doi.org/10.1016/j.ijms.2017.09.013.
[45] J. Zhen, D.M. Paardekooper, A. Candian, H. Linnartz, A.G.G.M. Tielens, Quadrupole ion trap/time-of-flight photo-fragmentation spectrometry of the hexaperi-hexabenzocoronene (HBC) cation, Chem. Phys. Lett. 592 (2014) 211–216, https://doi.org/10.1016/j.cplett.2013.12.005.
[46] N.A. Sassin, S.C. Everhart, J.I. Cline, K.M. Ervin, Photodissociation and collisional cooling of rhodamine 575 cations in a quadrupole ion trap, J. Chem. Phys. 128 (2008) 234305, https://doi.org/10.1063/1.2931553.
[47] K. Gulyuz, C.N. Stedwell, D. Wang, N.C. Polfer, Hybrid quadrupole mass filter/quadrupole ion trap/time-of-flight-mass spectrometer for infrared multiple photon dissociation spectroscopy of mass-selected ions, Rev. Sci. Instrum. 82 (2011), 054101, https://doi.org/10.1063/1.3585982.
[48] G. Wenzel, C. Joblin, A. Giuliani, S. Rodriguez Castillo, G. Mulas, M. Ji, H. Sabbah, S. Quiroga, D. Peña, L. Nahon, Astrochemical relevance of VUV ionization of large PAH cations, A&A 641 (2020) A98, https://doi.org/10.1051/0004-6361/202038139.
[49] V.M. Doroshenko, R.J. Cotter, Advanced stored waveform inverse Fourier transform technique for a matrix-assisted laser desorption/ionization quadrupole ion trap mass spectrometer, Rapid Commun. Mass Spectrom. 10 (1996) 65–73, https://doi.org/10.1002/(SICI)1097-0231(19960115)10:1<65::AID-RCM447>3.0.CO;2-M.
[50] G. Trinquier, A. Simon, M. Rapacioli, F.X. Gadéa, PAH chemistry at eV internal energies. 1. H-shifted isomers, Molecular Astrophysics 7 (2017) 27–36, https://doi.org/10.1016/j.molap.2017.02.001.
[51] T. Chen, M. Gatchell, M.H. Stockett, R. Delaunay, A. Domaracka, E.R. Micelotta, A.G.G.M. Tielens, P. Rousseau, L. Adoui, B.A. Huber, H.T. Schmidt, H. Cederquist, H. Zettergren, Formation of H $_2$ from internally heated polycyclic aromatic hydrocarbons: excitation energy dependence, J. Chem. Phys. 142 (2015) 144305, https://doi.org/10.1063/1.4917021.
[52] C.W. Bauschlicher, E. Peeters, L.J. Allamandola, The infrared spectra of very large irregular polycyclic aromatic hydrocarbons (PAHs): observational probes of astronomical PAH geometry, size, and charge, APJ (Acta Pathol. Jpn.) 697 (2009) 311–327, https://doi.org/10.1088/0004-637X/697/1/311.
[53] J. Zhen, D.M. Paardekooper, A. Candian, H. Linnartz, A.G.G.M. Tielens, Quadrupole ion trap/time-of-flight photo-fragmentation spectrometry of the hexaperi-hexabenzocoronene (HBC) cation, Chem. Phys. Lett. 592 (2014) 211–216, https://doi.org/10.1016/j.cplett.2013.12.005.
[54] P. Pla, C. Dubosq, M. Rapacioli, E. Posenitskiy, M. Alcamí, A. Simon, Hydrogenation of C_{24} carbon clusters: structural diversity and energetic properties, J. Phys. Chem. (2021), https://doi.org/10.1021/acs.jpca.1c02359.
[55] C. Dubosq, F. Calvo, M. Rapacioli, E. Dartois, T. Pino, C. Falvo, A. Simon, Quantum modeling of the optical spectra of carbon cluster structural families and relation to the interstellar extinction UV bump, A&A 634 (2020) A62, https://doi.org/10.1051/0004-6361/201937090.
[56] C. Dubosq, C. Falvo, F. Calvo, M. Rapacioli, P. Parneix, T. Pino, A. Simon,

Mapping the structural diversity of C_{60} carbon clusters and their infrared spectra, Astron. Astrophys. 625 (2019), https://doi.org/10.1051/0004-6361/201834943.
[57] B. West, F. Useli-Bacchitta, H. Sabbah, V. Blanchet, A. Bodi, P.M. Mayer, C. Joblin, Photodissociation of pyrene cations: structure and energetics from $C_{16}H_{10}^{+}$ to C_{14}^{+} and almost everything in between, J. Phys. Chem. A. 118 (2014) 7824−7831, https://doi.org/10.1021/jp506420u.
[58] G. Trinquier, A. Simon, M. Rapacioli, F.X. Gadéa, PAH chemistry at eV internal energies. 2. Ring alteration and dissociation, Molecular Astrophysics 7 (2017) 37−59, https://doi.org/10.1016/j.molap.2017.02.002.
[59] M. Gatchell, H. Zettergren, Knockout driven reactions in complex molecules and their clusters, J. Phys. B Atom. Mol. Opt. Phys. 49 (2016) 162001, https://doi.org/10.1088/0953-4075/49/16/162001.
[60] A. Simon, J.P. Champeaux, M. Rapacioli, P. Moretto Capelle, F.X. Gadéa, M. Sence, Dissociation of polycyclic aromatic hydrocarbons at high energy: MD/DFTB simulations versus collision experiments: fragmentation paths, energy distribution and internal conversion: test on the pyrene cation, Theor Chem Acc 137 (2018) 106, https://doi.org/10.1007/s00214-018-2287-z.
[61] T. Monfredini, H.M. Quitián-Lara, F. Fantuzzi, W. Wolff, E. Mendoza, A.F. Lago, D.A. Sales, M.G. Pastoriza, H.M. Boechat-Roberty, Destruction and multiple ionization of PAHs by X-rays in circumnuclear regions of AGNs, Mon. Not. Roy. Astron. Soc. 488 (2019) 451−469, https://doi.org/10.1093/mnras/stz1021.
[62] G. Reitsma, L. Boschman, M.J. Deuzeman, S. Hoekstra, R. Hoekstra, T. Schlathölter, Near edge X-ray absorption mass spectrometry on coronene, J. Chem. Phys. 142 (2015), 024308, https://doi.org/10.1063/1.4905471.
[63] C. Joblin, Carbon Macromolecules in the Cycle of Interstellar Matter: Observational and Laboratory Experiments, 2003. https://ui.adsabs.harvard.edu/abs/2003sf2a.conf..175J. (Accessed 23 November 2021). accessed.
[64] A. Candian, M. Gomes Rachid, H. MacIsaac, V.N. Staroverov, E. Peeters, J. Cami, Searching for stable fullerenes in space with computational chemistry, Mon. Not. Roy. Astron. Soc. 485 (2019) 1137−1146, https://doi.org/10.1093/mnras/stz450.
[65] T. Motylewski, H. Linnartz, O. Vaizert, J.P. Maier, G.A. Galazutdinov, F.A. Musaev, J. Krelowski, G.a.H. Walker, D.A. Bohlender, Gas-phase electronic spectra of carbon-chain radicals compared with diffuse interstellar band observations, Astrophys. J. 531 (2000) 312−320, https://doi.org/10.1086/308465.
[66] A. Omont, Interstellar fullerene compounds and diffuse interstellar bands, Astron. Astrophys. 590 (2016), https://doi.org/10.1051/0004-6361/201527685.
[67] A. Omont, H. Bettinger, Intermediate-size fullerenes as degradation products of interstellar polycyclic aromatic hydrocarbons, Astronomy and Astrophysics - A&A 650 (2021) A193, https://doi.org/10.1051/0004-6361/202140675.
[68] J.T. Buntine, M.I. Cotter, U. Jacovella, C. Liu, P. Watkins, E. Carrascosa, J.N. Bull, L. Weston, G. Muller, M.S. Scholz, E.J. Bieske, Electronic spectra of positively charged carbon clusters—C_{2n}^{+} ($n = 6$−14), J. Chem. Phys. 155 (2021) 214302, https://doi.org/10.1063/5.0070502.
[69] R. Nagarajan, J.P. Maier, Electronic spectra of carbon chains and derivatives, Int. Rev. Phys. Chem. 29 (2010) 521−554, https://doi.org/10.1080/0144235X.2010.490328.
[70] E.B. Jochnowitz, J.P. Maier, Electronic spectroscopy of carbon chains, Annu. Rev. Phys. Chem. 59 (2008) 519−544, https://doi.org/10.1146/annurev.physchem.59.032607.093558.
[71] P. Jenniskens, M. Gabadirwe, Q. Yin, A. Proyer, O. Moses, T. Kohout, F. Franchi, R.L. Gibson, R. Kowalski, E.J. Christensen, A.R. Gibbs, A. Heinze, L. Denneau, D. Farnocchia, P.W. Chodas, W. Gray, M. Micheli, N. Moskovitz, C.A. Onken, C. Wolf, H.A.R. Devillepoix, Q. Ye, D.K. Robertson, P. Brown, E. Lyytinen, J. Moilanen, J. Albers, T. Cooper, J. Assink, L. Evers, P. Lahtinen, L. Seitshiro, M. Laubenstein, N. Wantlo, P. Moleje, J. Maritinkole, H. Suhonen, M.E. Zolensky, L. Ashwal, T. Hiroi, D.W. Sears, A. Sehlke, A. Maturilli, M.E. Sanborn, M.H. Huyskens, S. Dey, K. Ziegler, H. Busemann, M.E.I. Riebe, M.M.M. Meier, K.C. Welten, M.W. Caffee, Q. Zhou, Q. Li, X. Li, Y. Liu, G. Tang, H.L. McLain, J.P. Dworkin, D.P. Glavin, P. Schmitt-Kopplin, H. Sabbah, C. Joblin, M. Granvik, B. Mosarwa, K. Botepe, J. Trigo-Rodríguez, The impact and recovery of asteroid 2018 LA, Meteoritics Planet Sci. 56 (2021) 844−893, https://doi.org/10.1111/maps.13653.
[72] L. Martínez, G. Santoro, P. Merino, M. Accolla, K. Lauwaet, J. Sobrado, H. Sabbah, R.J. Pelaez, V.J. Herrero, I. Tanarro, M. Agúndez, A. Martín-Jimenez, R. Otero, G.J. Ellis, C. Joblin, J. Cernicharo, J.A. Martín-Gago, Prevalence of non-aromatic carbonaceous molecules in the inner regions of circumstellar envelopes, Nat. Astron. 4 (2020) 97−105, https://doi.org/10.1038/s41550-019-0899-4.